Fluid simulations of toroidal ion temperature gradient turbulence

I. Sandberg[a)]
Department of Electrical and Computer Engineering, National Technical University of Athens, GR-157 73, Association Euratom—Hellenic Republic, Athens, Greece

H. Isliker
Department of Physics, Aristotle University of Thessaloniki, GR-541 24, Association Euratom—Hellenic Republic, Thessaloniki, Greece

V. P. Pavlenko
Department of Astronomy and Space Physics, Uppsala University, Box 515, SE-751 20, Euratom—VR Fusion Association, Uppsala, Sweden

K. Hizanidis
Department of Electrical and Computer Engineering, National Technical University of Athens, GR-157 73, Association Euratom—Hellenic Republic, Athens, Greece

L. Vlahos
Department of Physics, Aristotle University of Thessaloniki, GR-541 24, Association Euratom—Hellenic Republic, Thessaloniki, Greece

(Received 10 October 2005; accepted 9 January 2006; published online 21 February 2006)

The evolution of the toroidal ion temperature gradient mode instability is numerically studied by using the equations based on the standard reactive fluid model. The long-term dynamics of the instability are investigated using random-phase, small-amplitude fluctuations for initial conditions. The main events during the evolution of the instability that lead to the formation of large-scale coherent structures are described and the role of the dominant nonlinearities is clarified. The polarization drift nonlinearity leads to the inverse energy cascade while the convective ion heat nonlinearity is responsible for the saturation of the instability. Finally, the sensitivity of the saturated state to the initial plasma conditions is examined. © *2006 American Institute of Physics*.
[DOI: 10.1063/1.2171653]

I. INTRODUCTION

Low-frequency electrostatic turbulence driven by spatial gradients is believed to be the main source of anomalous transport in magnetically confined fusion plasmas.[1,2] During recent years, a significant number of both theoretical and numerical investigations in plasma dynamics have focused on the effects related to the development of the ion temperature gradient (ITG) mode instability.[3] This is due to the successful interpretations of various experimental results—elated to the observed levels of turbulent transport in tokamak plasmas—through the dynamics of the ITG mode. The associated instability appears due to the gradient of the ion temperature profile along the radial direction, and in tokamaks it is mainly driven by the magnetic field curvature.[4] There have been several descriptions of the toroidal ITG instability based on kinetic, gyrofluid, or fluid models. One suitable description is based on the so-called reactive fluid model,[5] which exhibits excellent agreement in the estimation of the ion heat diffusivity coefficient with full three-dimensional (3D) nonlinear gyrokinetic particle simulations.

Most of the models that are widely used to calculate the turbulent transport coefficients are based on the estimation of the mixing length. This approach has raised some questions since turbulence self-organizes through the nonlinearly self-generated structures and the dynamics of such complex systems cannot be described by a simple mixing length rule (see the review by Garbet[6]). Particular interest has been given to the anisotropic flows with additional symmetry, commonly known as zonal flows (ZF's), which are convective cells elongated in the poloidal direction; or streamers, which are convective cells elongated in the radial direction. In tokamaks, ZF's have the ability to limit the radial size of turbulent eddies through the shear decorrelation mechanism,[7] while streamers may lead to enhanced or bursty levels of transport.[8] Obviously, the formation of such anisotropic coherent structures is rather crucial as it determines the level of the energy transport in tokamak regimes of enhanced confinement.

Based on the reactive fluid model description, it has been shown[9,10] that resonant excitation of ZF's close to the marginal stability conditions can take place. Furthermore, numerical simulations[11,12] have investigated the stability and the interaction properties, respectively, of convective cells governed by the toroidal ITG equations. In these numerical studies, the authors imposed as initial conditions already formed convective cells.

In a recent work,[13] the explicit instability threshold of the toroidal ITG instability was determined by taking into account the finite Larmor radius (FLR) effects. It was shown that FLR effects may decrease significantly the instability threshold in regions of peaked plasma density and the associated marginally unstable modes attain finite wavelengths.

[a)]Electronic address: sandberg@central.ntua.gr

These consequences could be rather crucial regarding the properties of large-scale flows that are attributed to the development of the toroidal ITG instability near marginal conditions.

In the present paper, we investigate numerically the evolution of the toroidal ITG instability, choosing randomly phased small-amplitude fluctuations as initial conditions in contrast to Refs. 11 and 12, and we examine the properties of the temporal evolution of the instability, similar to our studies regarding flute turbulence.[14] Furthermore, we chose plasma conditions near marginally unstable conditions that allow us to investigate the sensitivity of the saturated state of the ITG instability to the wave number of the linearly most grown mode, which actually depends on the FLR effects. We focus on the long-term dynamics and in particular on the self-organization of the ITG turbulence, which is significant for the energy transport in tokamak plasmas.

As it turns out the temporal evolution of the toroidal ITG instability leads to a saturated stationary state which is characterized by the presence of long-lived coherent structures. The condensation of energy in such scales is commonly attributed to the inverse energy cascade properties of the polarization drift nonlinearity in a similar manner as in the adiabatic drift wave turbulence, as described by the Hasegawa-Mima equation. However, the nonlinear evolution of the ITG instability is also determined by the convective ion heat flux nonlinearity. Thus, in what follows we also investigate the separate role that each of the dominant nonlinearities plays in the evolution and the stabilization of the instability. Furthermore, the influence of the plasma parameters, of the dissipative effects, and of the wavelengths of the linearly unstable ITG modes on the saturated state is examined.

In Sec. II, we briefly present the model and the linear properties of the toroidal ITG instability, and in Sec. III we describe and investigate the properties of the evolution of the instability based on a series of numerical simulations. Lastly, in Sec. IV a summary and the conclusions of our study are given.

II. MODEL OF EQUATIONS

The 2D model equations that describe the dynamics of the toroidal ITG modes can be derived in the two-fluid plasma approximation[15] by using a low-frequency expansion based on the standard drift velocity ordering. The ion continuity and the ion temperature equations, respectively, can be written in the following normalized form:[9]

$$\frac{\partial n_i}{\partial t} - \left[\frac{\partial}{\partial t} - \tau(1+\eta_i)\frac{\partial}{\partial y}\right]\nabla_\perp^2\phi + \frac{\partial \phi}{\partial y} - \epsilon_n \frac{\partial}{\partial y}[\phi + \tau(n_i + T_i)] + \mu\nabla^2\nabla^2\phi = \{\phi, \nabla_\perp^2\phi - n_i\} \tag{1}$$

and

$$\frac{\partial T_i}{\partial t} - \frac{5}{3}\tau\epsilon_n\frac{\partial T_i}{\partial y} + \left(\eta_i - \frac{2}{3}\right)\frac{\partial \phi}{\partial y} - \frac{2}{3}\frac{\partial n_i}{\partial t} - D\nabla^2 T_i = \left\{\phi, \frac{2}{3}n_i - T_i\right\}. \tag{2}$$

Details on the derivation may be found in Ref. 5. The curly brackets on the right-hand side of Eqs. (1) and (2) denote the Poisson bracket, defined by $\{A,B\}=\partial_x A\partial_y B - \partial_x B\partial_y A$.

To close the system of equations, we assume that electrons follow the Boltzmann distribution and that the low-frequency electrostatic oscillations $\omega \ll \omega_{ci}$ are quasineutral, i.e.,

$$n_e = n_i = \phi. \tag{3}$$

The length and the time scales have been normalized by $\rho_s = c_s/\omega_{ci}$ and L_n/c_s, respectively, where $c_s^2 = T_e/m_i$ is the ion sound velocity defined at the electron temperature, $\omega_{ci} = eB_0/m_i c$ is the ion gyrofrequency, and $L_g^{-1} = -d\ln g(r)/dr$ describes the inverse characteristic scale length of inhomogeneity along the radial direction of the plasma parameter $g(r)$, where $g(r)=n(r)$, $T_i(r)$. The electrostatic potential $\delta\phi$ has been normalized as $\phi = e\delta\phi/T_e\, L_n/\rho_s$, the perturbed density δn as $n = \delta n/n_0\, L_n/\rho_s$, and the perturbed ion temperature δT_i as $T_i = \delta T_i/T_{i0}\, L_n/\rho_s$. With the curvature R of the magnetic field lines and the ion temperature inhomogeneity scale length L_{T_i}, we define $\epsilon_n = 2L_n/R$ and $\eta_i = L_n/L_{T_i}$, respectively, where L_n is the plasma inhomogeneity scale length. Furthermore, $\tau = T_i/T_e$ denotes the ratio of ion to electron temperature, while μ and D are the viscosity and the diffusion coefficients, respectively. We point out that effects attributed to parallel ion dynamics, magnetic shear, electron particle trapping, Landau damping, plasma shape, and finite beta[16] are omitted.

We should point out here that the model of equations is invalid for the description of flute (or interchange) type modes as the Boltzmann relation is invalid for $k_\parallel = 0$. The inclusion of flute type modes can be realized numerically by performing a three-dimensional fluid simulation, and by using the electron continuity equation for the $k_\parallel = 0$ modes. Thus, the description and the results presented in this article are valid only for modes with finite parallel wave numbers. This slightly limiting approach is actually well justified for the description of the modes with finite $k_\parallel$ and has been widely used for many drift–type modes.

The dispersion relation for the toroidal ITG instability can be determined by the linearization of Eqs. (1)–(3) and by applying the Fourier expansion $\propto \exp(-i\omega t + \mathbf{k}\cdot\mathbf{r})$ to the perturbed quantities, where $\mathbf{r}$ and $\mathbf{k}$ are the position vector and the wave number of the perturbation, respectively. In the following, we briefly present the results of Ref. 13 for the ideal case $\mu = D = 0$.

The real frequency $\omega(\mathbf{k}_\perp)$ and the growth rate $\gamma(\mathbf{k}_\perp)$ of the toroidal ITG mode are given by

$$\omega_k^{\mathrm{RE}} = \frac{k_y}{2(1+k_\perp^2)}\left\{1-\epsilon_n-\frac{10}{3}\epsilon_n\tau - \left[\tau(1+\eta_i)+\frac{5}{3}\tau\epsilon_n\right]k_\perp^2\right\} \tag{4}$$

and

$$\gamma_k = \frac{k_y}{2(1+k_\perp^2)}\sqrt{f(k_\perp^2)}. \tag{5}$$

The radical $f(k_\perp^2)$ in Eq. (5) has the form

$$f(k_\perp^2) = 4\epsilon_n\tau(\eta_i-\eta_C)+2\tau(1+\epsilon_n)(\eta_i-\eta_B)k_\perp^2 - \tau^2\left(1+\eta_i-\frac{5}{3}\epsilon_n\right)^2 k_\perp^4, \tag{6}$$

where the parameters η_B and η_C are

$$\eta_B = \frac{4\epsilon_n-1}{\epsilon_n+1}-\frac{5}{3}\frac{\epsilon_n^2}{\epsilon_n+1}\left(1-\frac{4}{3}\tau\right) \tag{7}$$

and

$$\eta_C = \frac{2}{3}+\frac{10}{9}\epsilon_n\tau+\frac{(\epsilon_n-1)^2}{4\epsilon_n\tau}. \tag{8}$$

From Eqs. (5)–(8) it turns out that the toroidal ITG modes become unstable for $\eta_i > \eta_{ith}$ and the explicit threshold η_{ith} for the instability is found to be[13]

$$\eta_{ith}(\epsilon_n,\tau) = \begin{cases} \eta_* & \text{for } \epsilon_n<1, \text{ and for } \epsilon_n>1 \text{ when } 0<\tau<\tau_*, \\ \eta_C & \text{for } \epsilon_n>1 \text{ when } \tau>\tau_*\equiv 3(1-1/\epsilon_n)/2, \end{cases} \tag{9}$$

where

$$\eta_* = \frac{2}{3}+\frac{10}{9}\epsilon_n\tau. \tag{10}$$

Further analysis shows that the wave number of the marginal unstable mode, i.e., $\gamma(k_{\perp m})=0$, is equal to

$$k_{\perp m}^2 \simeq \begin{cases} \dfrac{(1+\epsilon_n)(\eta_i-\eta_B)}{\tau\left(1+\eta_i-\frac{5}{3}\epsilon_n\right)^2}, & \text{when } \eta_{ith}=\eta_*, \text{ and} \\ 0, & \text{when } \eta_{ith}=\eta_C. \end{cases} \tag{11}$$

The threshold of the instability was previously given by η_C without taking into account the FLR effects, e.g., in Ref. 5. However, for $\epsilon_n<1$ the FLR effects become rather important,[13] leading to a decrease of the threshold and to the appearance of the marginal unstable modes at a shorter wavelength regime. As a consequence, for $\eta_*<\eta_i<\eta_C$ there is a stable region in the wavelength regime around $k_\perp=0$. These results are crucial for the self-generation of large-scale flows by the toroidal ITG turbulence since they establish new marginal conditions for the release of the available free energy, which is necessary for the formation of large-scale flows.

III. NUMERICAL RESULTS

In this section, we numerically study the linear and nonlinear temporal evolution of the toroidal ITG modes described by the model Eqs. (1)–(3). We use a dealiased pseudospectral code in a numerical grid of 128×128 points. The marching in time is performed with a fourth-order Runge-Kutta technique with adaptive step size. We have imposed periodic boundary conditions and considered a physical domain in the $x-y$ plane of area $\Delta x\times\Delta y=[(-30\pi,30\pi)\times(-30\pi,30\pi)]$. The minimum finite wave number that can be resolved with our scheme is $k_0=k_{x0}=k_{y0}=0.033$. The initial conditions for the potential and temperature perturbations consist of an *isotropic spectrum* of small-amplitude and randomly phased Fourier modes of the form

$$\phi(x,y)=\sum_{k_x}\sum_{k_y}\hat{\phi}\exp(i\vec{k}\cdot\vec{r}+i\alpha_{k_x,k_y}),$$

$$T(x,y)=\sum_{k_x}\sum_{k_y}\hat{T}\exp(i\vec{k}\cdot\vec{r}+i\beta_{k_x,k_y}),$$

where $\hat{\phi}=0.001$, $\hat{T}=0.0001$, and $\alpha_{k_x,k_y},\beta_{k_x,k_y}$ are randomly generated initial phases.

A. Dynamics of toroidal ITG instability

In what follows, we describe the main parts of the evolution of the toroidal ITG instability based on the numerical integration of Eqs. (1)–(3). Furthermore, we investigate the particular role that each nonlinearity plays in the transfer of energy between the modes. Throughout this subsection, we use the values $\eta_i=1.02\eta_*$, $\epsilon_n=1$, $\tau=1$, and $\mu=0.2$, which can be characterized as typical plasma parameters in tokamaks.

Linear excitation of the ITG modes. The first phase of the evolution of the ITG instability is characterized by the excitation and growth of the linearly unstable modes. During this phase, radial patterns of the fluctuating potential and temperature are formed that propagate along the poloidal direction with their characteristic group velocity. In Fig. 1(a), a snapshot of the potential fluctuations is plotted, at $t=90$, which shows the characteristic radial patterns attributed to the linear evolution of the instability. The amplitudes of the corresponding Fourier modes are presented in Fig. 2(a) for the same time. The highest amplitudes correspond to the fastest growing unstable modes, which are localized around wave number $k_{\mathrm{linear}}\simeq k_y\simeq0.4$ and have growth rate $\gamma\simeq0.07$ for the chosen plasma parameters, in agreement with Eqs. (5), (6), and (11), as expected.

Onset of nonlinear effects. When the amplitudes of the perturbations reach a critical value, the nonlinear interactions between the modes become important and modify drastically the form of the electrostatic fluctuations. The onset of nonlinear effects appears with a sudden excitation of a wide range of modes which follow the inequality $0<k_\perp^2<k_{\mathrm{linear}}^2$. The growth of these modes is attributed to the inverse cascade of the energy stored in the linearly grown modes. In Fig. 2(b), the spectrum of the ITG modes is presented right after the collapse of the linear regime, where it is seen that the nonlinearities tend first to isotropize the spectra. In Fig. 1(b), we see that the energy spread leads to the breaking of

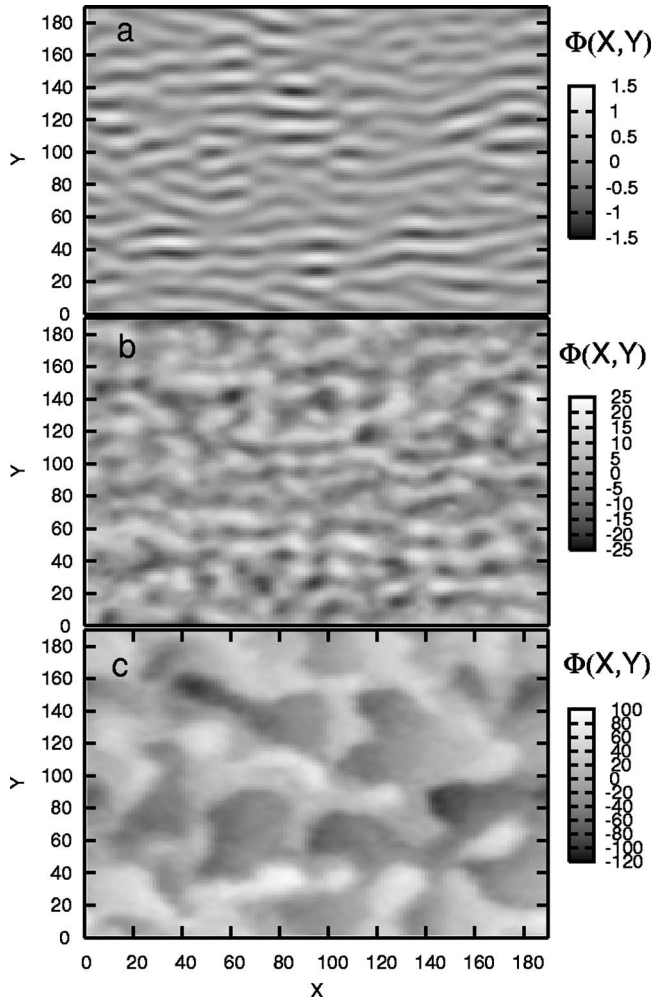

FIG. 1. Profiles of the fluctuating electrostatic potential during the development and saturation of the toroidal ITG instability for (a) $t=90$, (b) $t=190$, and (c) $t=990$. The chosen plasma parameters for this simulation were $\epsilon_n=\tau=1$, $\eta_i=1.02\eta_*$, $\mu=0.2$, and $D=0$. As initial conditions ($t=0$) random-phase noise fluctuations were chosen.

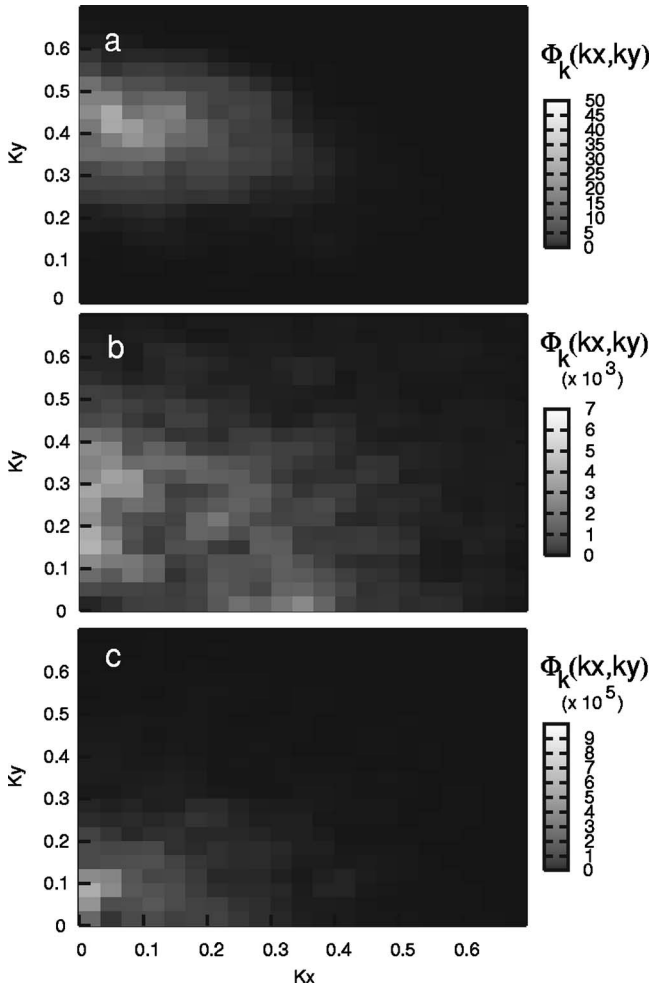

FIG. 2. The Fourier spectra of the fluctuating electrostatic potential during the development and saturation of the toroidal ITG instability for the same times and plasma parameters as in Fig. 1.

the radial patterns and to a subsequent formation of short-scale intermediate structures. Later on, the nonlinear effects lead to a condensation of the energy toward the large-scale modes.

Saturated state of ITG turbulence. The inverse energy cascade continues until the system reaches a turbulent stationary state, which is characterized by the existence of large-scale coherent structures slightly elongated along the radial direction [see Fig. 1(c)]. This is also evident in the Fourier spectra [see Fig. 2(c)], where it can be seen that modes of the type $\mathbf{k}(0,k_y \ll k_{\text{linear}})$, say streamer-type modes, have accumulated larger amplitudes compared to the modes of the type $\mathbf{k}(k_x \ll k_{\text{linear}},0)$, say zonal type modes.

The saturation mechanism occurs due to the nonlinearly excited modes, which suppress the toroidal ITG instability. The latter is responsible for the nonlinear excitation of the longer scales, and when it becomes suppressed, the growth of the larger scales is suppressed as well.

It should be mentioned here that during the turbulent stationary state, the onset of a secondary development and suppression of the linearly most unstable modes was observed. This results in the increase of the level of energy (see Fig. 7), without changing the overall picture of the fluctuations of the potential.

1. Investigation of the role of the nonlinear terms

The inverse energy cascade mechanism is commonly attributed to the polarization drift nonlinearity $\{\phi,\nabla_\perp^2\phi\}$, as in the drift-wave turbulence described by the Hasegawa-Mima model equation. However, in our case there is also the convective ion heat flux nonlinearity $\{\phi,T_i\}$, which appears in the ion temperature equation and is expected to modify significantly the cascade properties of the drift-type electrostatic turbulence.

In order to shed some light on the role that each Poisson-bracket nonlinearity plays in the evolution of the ITG instability, we have made two separate numerical runs for the same plasma parameters by keeping each time only one nonlinearity. In Fig. 3, the fluctuations of the potential are plotted for the same time ($t=340$) under the influence of different nonlinear interactions. In Fig. 3(a), the fluctuations are presented when Eqs. (1)–(3) are considered in their original form, which corresponds to the case described in the previous subsection.

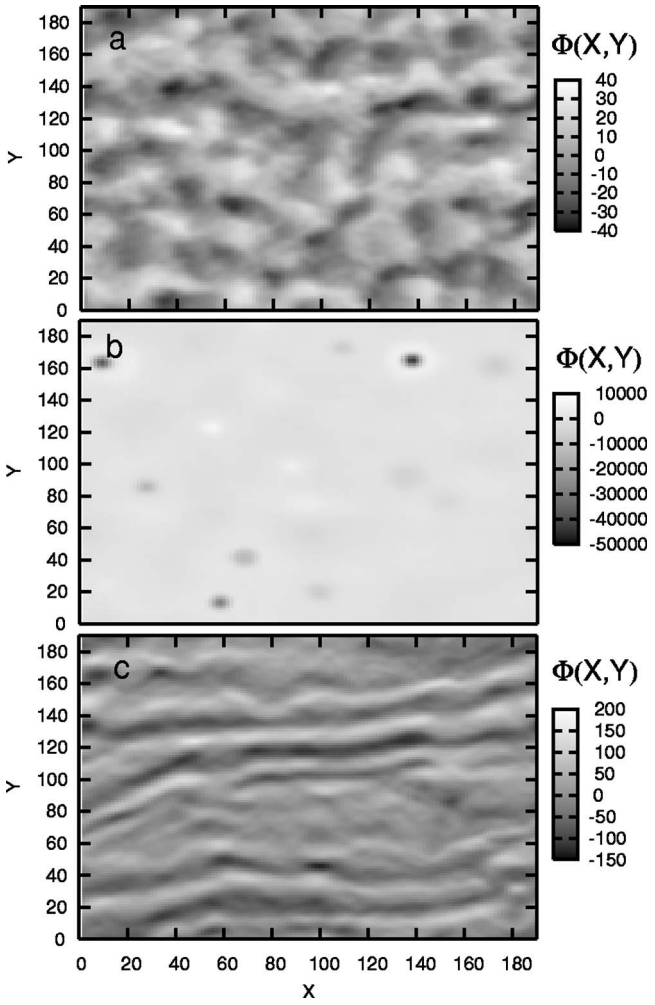

FIG. 3. Profiles of the fluctuating electrostatic potential at $t=340$ under the influence of different types of nonlinearities. (a) Both $\{\phi,\nabla_\perp^2\phi\}$ and $\{\phi,T_i\}$ included, (b) only the $\{\phi,\nabla_\perp^2\phi\}$ term, and (c) only the $\{\phi,T_i\}$ term included. The plasma parameters applied are the same as in Fig. 1.

The initial part of the evolution of Eqs. (1)–(3) under the sole influence of the polarization drift nonlinearity $\{\phi,\nabla_\perp^2\phi\}$ is qualitatively similar to the initial phase of the nonlinear evolution in the original problem. The sudden transfer of energy toward larger scales takes place as before [similar to Fig. 2(b)]. However, after some time the cascade does not continue further toward the largest scales as in the complete problem. Instead, a strong nonlinear instability with characteristic wave number smaller than k_{linear} is developed resulting in the appearance of short-scale spikes of the potential which grow fast, attaining very large amplitudes [see Fig. 3(b)]. This instability does not become suppressed and as a result the system does not reach any saturated state.

On the other hand, the evolution of Eqs. (1)–(3) under the sole influence of the ion heat flux nonlinearity $\{\phi,T_i\}$ leads to the suppression of the linear instability, and the resulting saturated state here is characterized by the presence of large-scale structures slightly elongated along the radial direction [see Fig. 3(c)].

The radially elongated structures in the saturated state are due to the suppression of the ITG linearly unstable modes under the sole influence of the ion heat flux nonlinearity. The resulting anisotropy is not attributed to the isotropic nonlinear term but to the anisotropy of the linearly unstable spectra and particularly to the fact that the most unstable modes are those with $k_x \simeq 0$. This effect does not appear in the presence of the polarization drift nonlinearity, as the $\{\Phi,\nabla^2\Phi\}$ term leads to an inverse spread of energy toward both poloidal and radial directions [see Fig. 2(b)] prior to the suppression, which is attributed to the $\{\phi,T_i\}$ nonlinearity.

These results are useful to explain the evolution of the toroidal ITG instability and demonstrate the importance of the synergetic role of the nonlinearities. Hence, we conclude that the nonlinear term $\{\phi,\nabla_\perp^2\phi\}$ is responsible for the energy spread toward the range of larger-scale modes. On the other hand, the nonlinear term $\{\phi,T_i\}$ is the one that provides the suppression mechanism against the instabilities, leading the system to a saturated state that is characterized by slightly radially elongated coherent structures.

B. Properties of the stationary saturated state of ITG turbulence

1. Anisotropy

In this subsection, we investigate the anisotropy of the turbulent spectra, and particularly the regime associated with large-scale anisotropic modes that are responsible for the formation of anisotropic flows with additional symmetry (zonal flows, streamers). In contrast to the saturated state of the magnetic-curvature-driven flute instability, where the largest anisotropic modes dominate,[14] the saturated state of the toroidal ITG instability is characterized by the coexistence of a significant number of dominant large-scale modes.

In order to quantify the characteristics of the anisotropy, we investigate the evolution of the ratios $\langle k_y^2\rangle/\langle k_x^2\rangle \equiv \Sigma_{k_x,k_y} k_y^2|\Phi(k_x,k_y)|^2/\Sigma_{k_x,k_y} k_x^2|\Phi(k_x,k_y)|^2$ and $\langle L_y^2\rangle/\langle L_x^2\rangle \equiv \Sigma_{k_x,k_y} k_y^{-2}|\Phi(k_x,k_y)|^2/\Sigma_{k_x,k_y} k_x^{-2}|\Phi(k_x,k_y)|^2$, which are useful indices to describe the short- and large-scale anisotropy of the ITG spectra, respectively. Furthermore, we track the evolution of the ratios $\langle k_{y0}^2\rangle/\langle k_{x0}^2\rangle \equiv \Sigma_{k_x,k_y} k_y^2|\Phi(0,k_y)|^2/\Sigma_{k_x,k_y} k_x^2|\Phi(k_x,0)|^2$ and $\langle L_{y0}^2\rangle/\langle L_{x0}^2\rangle \equiv \Sigma_{k_x,k_y} k_y^{-2}|\Phi(0,k_y)|^2/\Sigma_{k_x,k_y} k_x^{-2}|\Phi(k_x,0)|^2$, which give information on the relative energy deposited in the "purely" anisotropic short- and large-scale modes, respectively.

In Fig. 4(a), we present the evolution of the ratios $\langle L_y^2\rangle/\langle L_x^2\rangle$ and $\langle L_{y0}^2\rangle/\langle L_{x0}^2\rangle$, which describe the anisotropy in the large scales, and in Fig. 4(b) the evolution of $\langle k_y^2\rangle/\langle k_x^2\rangle$, $\langle k_{y0}^2\rangle/\langle k_{x0}^2\rangle$, which describes the short-scale anisotropy. The linear phase terminates around $t\sim 90$, when the nonlinear effects start to dominate, driving the system into a saturated state around $t\sim 190$. It can be seen that there is an isotropic spread of the energy between the modes that have finite wave numbers in both directions (i.e., those with $k_x k_y \neq 0$) as the corresponding ratios approach unity for $t>190$. However, this is not true for the purely anisotropic large-scale modes (i.e., those with $k_x k_y=0$) as the index $\langle L_{y0}^2\rangle/\langle L_{x0}^2\rangle$, which describes the ratio of energy between these modes, is larger than unity. In other words, the large-scale modes with $k_x=0$ possess larger energy compared to those with $k_y=0$ [see Figs.

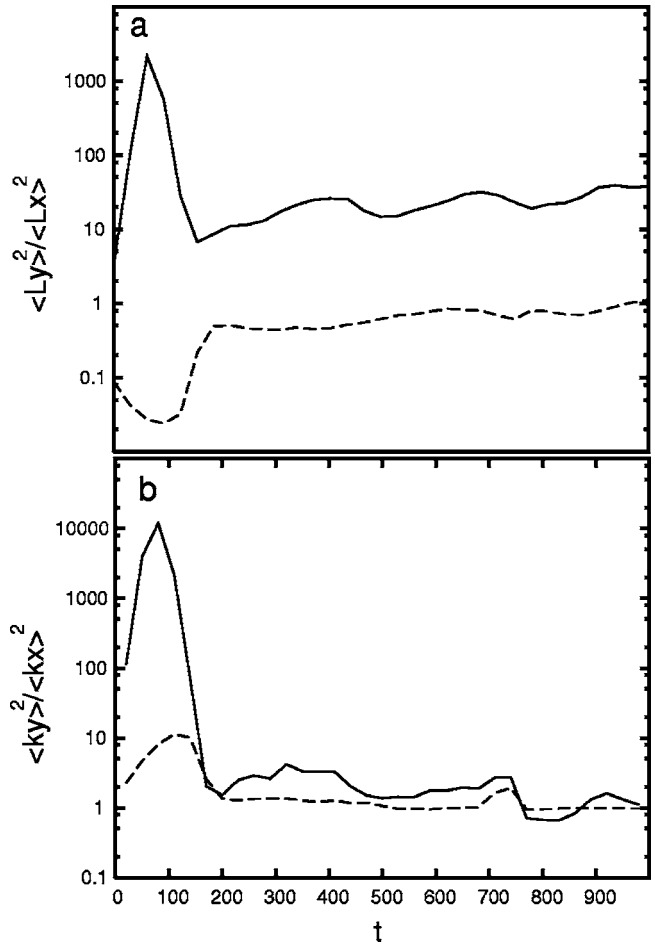

FIG. 4. Evolution of the characteristic anisotropy indices. In the upper panel, the large-scale ratios $\langle L_y^2\rangle/\langle L_x^2\rangle$ (dashed line) and $\langle L_{y0}^2\rangle/\langle L_{x0}^2\rangle$ (solid line) are plotted. In the lower panel, the short-scale ratios $\langle k_y^2\rangle/\langle k_x^2\rangle$ (dashed line) and $\langle k_{y0}^2\rangle/\langle k_{x0}^2\rangle$ (solid line) are plotted. In the saturated state, all the indices approach unity (isotropy) apart from the index $\langle L_{y0}^2\rangle/\langle L_{x0}^2\rangle$. The plasma parameters we have used are the same as in Fig. 1.

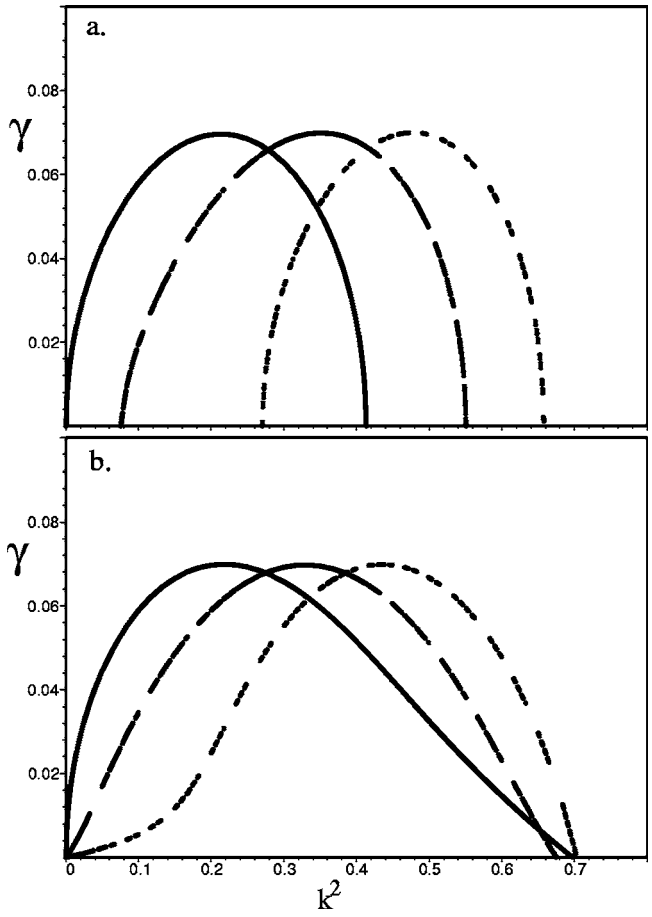

FIG. 5. Growth rates of linearly unstable modes for dissipationless (upper panel) and dissipative (lower panel) cases. The solid lines corresponds to $\epsilon_n=1$, where $\eta_i/\eta_*=1.0225$ for the upper panel and $\eta_i/\eta_*=1.0261$ for the lower panel. Similarly, the long dashed lines corresponds to $\epsilon_n=0.6$, where $\eta_i/\eta_*=1.025$ for the upper panel and $\eta_i/\eta_*=1.0366$ for the lower panel, and the dashed lines correspond to $\epsilon_n=0.3$, where $\eta_i/\eta_*=1.0515$ for the upper panel and $\eta_i/\eta_*=1.099$ for the lower panel. Furthermore, $\mu=D=0$ (upper panel) and $\mu=D=0.1$ (lower panel), and $\tau=1$.

2(b) and 2(c)]. This is also reflected in the slight elongation of the coherent structures along the radial direction [see Fig. 1(c)].

In numerical runs where we kept solely the nonlinear term $\{\phi,\nabla_\perp^2\phi\}$, the relation $\langle L_{x0}^2\rangle\sim\langle L_{y0}^2\rangle$ holds instead, showing the isotropy of the amplitudes of the modes. On the other hand, when we kept only the nonlinear term $\{\phi,T_i\}$, the inequalities $\langle k_{x0}^2\rangle\ll\langle k_{y0}^2\rangle$ and $\langle k_{x0}^{-2}\rangle\ll\langle k_{y0}^{-2}\rangle$ held during the evolution of the ITG instability. These results verify the conclusions about the role of the nonlinear terms as reported in the previous subsection.

2. Effects associated with the linearly unstable spectra

In order to investigate the effect of the plasma parameters on the turbulent saturated spectra, we have made several numerical runs, choosing different parameters that correspond to different linearly unstable spectra. This leads to a modification of the characteristic wave number at which the available free energy is pumped into the system.

In particular, we modified the inhomogeneity scale length ϵ_n for the general case in which ion and electron temperatures are equal. For each ϵ_n we chose a value of η_i such that the growth rate of the most unstable mode is equal to $\gamma=0.7$. In Fig. 5(a), we present the growth rates $\gamma(k)$ of three different linearly unstable spectra (for the purely poloidal propagation, i.e., $k_x=0$) for the dissipationless limit $\mu=D=0$, while in Fig. 5(b), we present similar cases for the dissipation limit $\mu=D=0.1$.

When μ and D are introduced, the linear growth rates $\gamma(k)$ change. In particular, the presence of D leads to a small widening of the linear growth rate spectra toward short and large wave numbers. On the other hand, the presence of μ leads to a small widening toward the small wave numbers. Furthermore, both μ and D suppress the growth rates of the most unstable modes. It is worthwhile to mention here that the modification of the plasma parameters ϵ, τ, η, μ, and D does not modify the nonlinear terms in Eqs. (1) and (2) as the parameters have been absorbed by the chosen normalization.

In all the numerical runs we performed, the qualitative characteristics of the temporal evolution of the toroidal ITG instability remain the same as described in the previous subsection. A main result of the comparison between the differ-

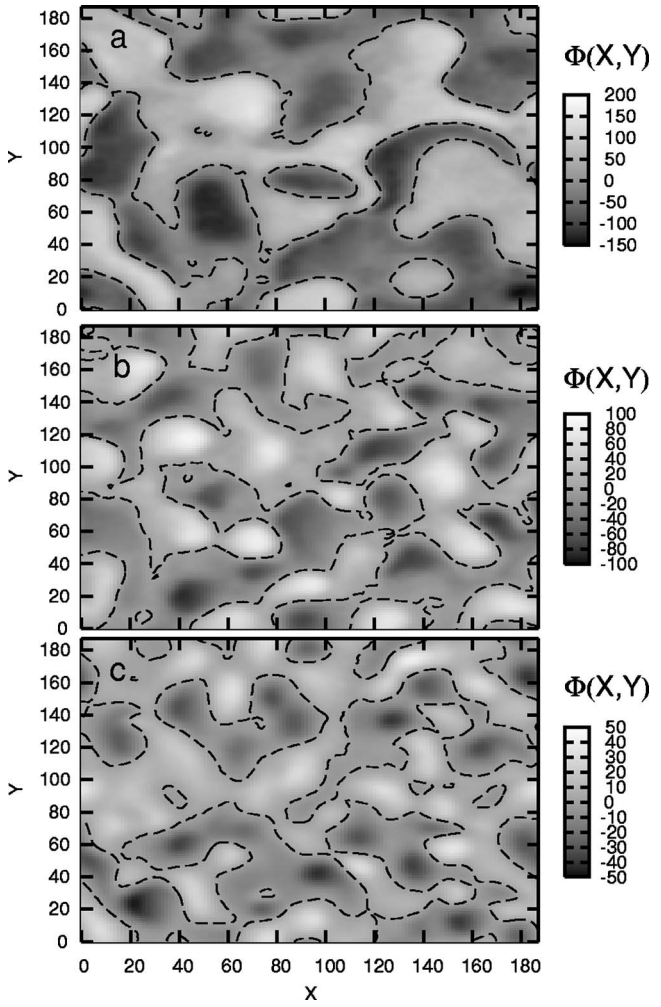

FIG. 6. Profiles of the saturated fluctuating electrostatic potential at $t=990$. The parameters we have used correspond to the linearly unstable spectra of Fig. 5(b), i.e., the dissipative case. (a) $(\epsilon_n, \eta_i/\eta_*)=(1, 1.0261)$ (upper panel), (b) $(\epsilon_n, \eta_i/\eta_*)=(0.6, 1.0366)$ (middle panel), and (c) $(\epsilon_n, \eta_i/\eta_*)=(0.3, 1.099)$ (lower panel).

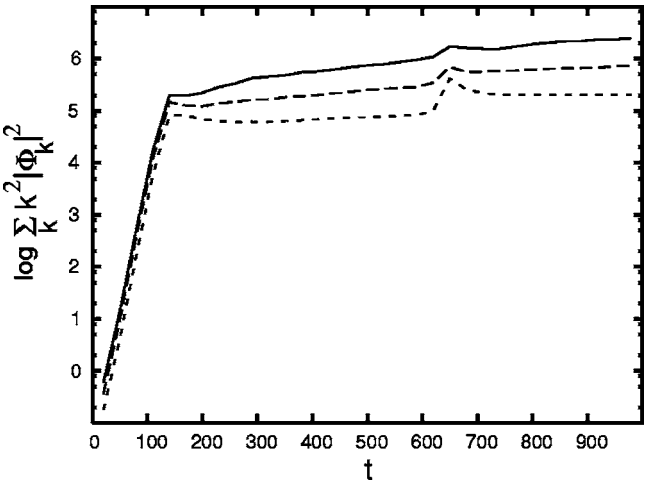

FIG. 7. Plots of the evolution of the energy $\Sigma_k k_\perp^2 |\Phi_k|^2$ for the initially linearly unstable ITG spectra of Fig. 5(b): (a) $(\epsilon_n, \eta_i/\eta_*)=(1, 1.0261)$ (solid line), (b) $(\epsilon_n, \eta_i/\eta_*)=(0.6, 1.0366)$ (dashed line), and (c) $(\epsilon_n, \eta_i/\eta_*)=(0.3, 1.099)$ (dotted line). The peak around $t=640$ corresponds to the onset of a secondary development of linearly unstable toroidal ITG modes.

ent numerical simulations concerns the size of the long-lived coherent structures, which are formed during the nonlinear phase of the evolution of the instability and persist in the saturated state. In particular, as the wavelength of the most linearly unstable mode increases, the size of the formed coherent structures also increases. This conclusion was verified in both dissipative (see Fig. 6) and dissipationless cases and indicates that the position of the peak in the linearly unstable spectra influences the characteristic coherency length in the stationary saturated state of toroidal ITG turbulence.

In Fig. 7, we have plotted the evolution of the electrostatic energy of the fluctuations for the three different sets of plasma parameters as presented in Fig. 5(b). The suppression of the linear instability takes place at lower levels of energy as the wave number of the most grown mode gets larger, and as a result the energy of the electrostatic fluctuations in the stationary turbulent state increases. From the definition of $\Sigma k^2 |\Phi_k|^2$ one would expect the opposite. A possible explanation lies in the fact that the number of modes that are nonlinearly excited gets larger as the wavelength of the linearly unstable mode increases (due to the inverse energy cascade). Since the nonlinearly generated modes are those responsible for the saturation of the system, the suppression mechanism is expected to become more effective as the number of these modes increases.

In all the comparative studies we did, we noticed that the amplitudes of the short-wavelength modes in the saturated state were significantly smaller in the presence of dissipative effects. At the same time, the amplitudes of the dominant large-scale modes were higher or at least comparable to those in the corresponding dissipationless cases. This was especially true for the large-scale anisotropic poloidal modes resulting in a further weakening of the radial elongation of the coherent structures. So, increasing gradually the diffusion coefficient D, we notice that the ratio $\langle L_{y0}^2 \rangle / \langle L_{x0}^2 \rangle$ approaches unity, showing a tendency for isotropy between the large-scale anisotropic modes. Furthermore, the energy level of the saturated electrostatic fluctuations $\Sigma k^2 |\Phi_k|^2$ was decreasing. This can be attributed to the suppression of the growth rates in the presence of D.

The same conclusions can be drawn from the comparisons of the characteristic autocorrelation length along the radial and poloidal directions, determined from the autocorrelation function of the turbulent fluctuations of the potential.

IV. CONCLUSIONS

The properties of the toroidal ITG instability have been investigated. The synergetic role of the polarization drift nonlinearity, which is responsible for the inverse energy cascade, and of the ion heat flux nonlinearity, which is responsible for the suppression of the instability, on the evolution and saturation of the toroidal ITG instability was reported. It becomes evident that the inverse energy cascade attributed to the nonlinear effects does not lead necessarily to the domination of the largest possible modes in the simulation box. The obtained results shows that as the wave number of the fastest growing linearly unstable mode decreases, (a) the size of the coherent structures in the stationary turbulent state

increases and (b) the amplitude of the fluctuations of the potential and the energy level increases. These results indicate that large-scale transport events attributed to the self-generated structures in toroidal ITG turbulence could be enhanced as the wavelength of the linear mode increases. Thus, the adjustment of the linearly unstable spectra through the control of plasma profiles might affect ITG turbulent transport. Furthermore, it is seen that dissipative effects weaken the radial elongation of the coherent structures.

ACKNOWLEDGMENTS

The authors are thankful to the anonymous referee for his/her useful remarks and suggestions, which enabled the improvement of the present article.

This work was supported under the Contract of Association ERB 5005 CT 99 0100 between the European Atomic Energy Community and the Hellenic Republic. The sponsors do not bear any responsibility for the contents in this work.

[1] W. Horton, Rev. Mod. Phys. **71**, 735 (1999).
[2] P. W. Terry, Rev. Mod. Phys. **72**, 109 (2000).
[3] L. I. Rudakov and R. Z. Sagdeev, Sov. Phys. Dokl. **6**, 415 (1961).
[4] B. Coppi and F. Pegoraro, Nucl. Fusion **17**, 969 (1977).
[5] J. Weiland, *Collective Modes in Inhomogeneous Plasmas* (IOP Publishing, Bristol, 2000).
[6] X. Garbet, Plasma Phys. Controlled Fusion **43**, A251 (2001).
[7] H. Biglari, P. H. Diamond, and P. W. Terry, Phys. Fluids B **2**, 1 (1990).
[8] P. Beyer, S. Benkadda, X. Garbet, and P. H. Diamond, Phys. Rev. Lett. **85**, 4892 (2000).
[9] J. Andersson, H. Nordman, R. Singh, and J. Weiland, Phys. Plasmas **9**, 4500 (2002).
[10] S. Dastgeer, S. Mahajan, and J. Weiland, Phys. Plasmas **9**, 4911 (2002).
[11] S. Dastgeer, IEEE Trans. Plasma Sci. **31**, 191 (2000).
[12] S. Dastgeer, J. Weiland, and S. Mahajan, Phys. Plasmas **9**, 4500 (2002).
[13] I. Sandberg, Phys. Plasmas **12**, 050701 (2005).
[14] I. Sandberg, H. Isliker, V. P. Pavlenko, K. Hizanidis, and L. Vlahos, Phys. Plasmas **12**, 032503 (2005).
[15] S. I. Braginskii, in *Reviews of Plasma Physics*, edited by M. A. Leontovich (Consultants Bureau, New York, 1965), Vol. 1.
[16] B. Jhowry, J. Andersson, and S. Dastgeer, Phys. Plasmas **11**, 5565 (2004).